Wall-function treatment in pdf methods for turbulent flows

Thomas D. Dreeben and Stephen B. Pope
Sibley School of Mechanical and Aerospace Engineering, Cornell University, Ithaca, New York 14853

(Received 17 January 1997; accepted 9 May 1997)

A wall-function boundary condition is developed for the pdf/Monte Carlo method. Like traditional wall functions, this reproduces the logarithmic velocity profile and shear stress in equilibrium flow conditions. A constant-stress analysis for the pdf, and a linear-stress analysis for the first two moments of the pdf are developed as the basis for this wall-function approach. Stable and accurate boundary conditions are derived and demonstrated with fully-developed channel flow. © *1997 American Institute of Physics.* [S1070-6631(97)01409-8]

I. INTRODUCTION

The effect of a solid wall on a turbulent flow is inherently difficult to model, because the flow includes strong inhomogeneity and anisotropy in the viscous sublayer adjacent to the wall. One computational approach to handling this is to impose a boundary condition at a point which corresponds to the inertial sublayer. The term ''wall functions'' has been applied to various forms of wall boundary conditions of this sort. Their purpose is to impose a boundary condition whose effect upon the overall flow is consistent with that of a wall, without characterizing the complex details of the flow in the near-wall region. They avoid the computational expense which is required to resolve the steep gradients of statistics which appear in the viscous sublayer. In spite of the widespread use of wall functions in turbulence closures, there has been no systematic development of such an approach with the pdf method. They have been developed and used for eddy-viscosity models,[1–4] for Reynolds-stress closures,[5,6] and incorporated once with the pdf method.[7] They are based on experimental results which have been found to be reasonably robust for flow in channels, pipes, and boundary layers:[8–10] In the inertial sublayer, the profile of mean velocity is a logarithmic function of the wall-normal distance y, the dissipation varies inversely with y, and the production and dissipation of turbulent kinetic energy are approximately equal to one another.

Wall functions are a method of imposing a boundary condition on a turbulent flow calculation which is consistent with the above observations. In that spirit, we develop the wall function with a model for the joint pdf of velocity and turbulent frequency. For velocity, we use the simplified Langevin model, which (apart from transport terms) is equivalent to Rotta's model. Accordingly, we aim to impose a condition which adequately reproduces the wall shear stress, as well as the profiles of velocity, turbulent kinetic energy, and dissipation, for moderate to large Reynolds numbers.

Wall-function boundary conditions are developed here with the currently standard and simplest possible pdf model formulation. In Section II we describe the relevant details of this Simplified Langevin model, its associated model for turbulent frequency, and their relationship to Reynolds-stress closures. In Section III we describe two different characterizations of the logarithmic layer, one standard analysis in which all the stresses are presumed to be independent of y, and another in which some of the less plausible assumptions are relaxed. The wall functions developed here draw heavily from ideas embodied in these analyses. In Section IV, we develop the boundary condition on each particle property. And in Section V, we show how these particle conditions work for fully-developed channel flow with a comparison to DNS data and to experimental results. Adequate agreement is achieved close to the wall, but modifications of the time-scale modeling are necessary to improve the velocity profile close to the channel halfplane. Results are shown both with and without the modifications.

II. BASIC MODEL

We develop the particle wall-function approach with the simplified Langevin model[11] in sufficient detail to allow for consistent extension to more complicated pdf models.

A. Pdf formulation

Let $\mathbf{U}(\mathbf{x},t)$ and $\mathscr{P}(\mathbf{x},t)$ be the Eulerian velocity and pressure, respectively, with Reynolds decompositions,

$$U_i = \langle U_i \rangle + u_i , \tag{1}$$

$$\mathscr{P} = \langle \mathscr{P} \rangle + p . \tag{2}$$

Let $\hat{f}(\mathbf{V};\mathbf{x},t)$ be the Eulerian pdf of velocity at a given location. The model formulation is an effort to close the exact pdf evolution equation for turbulent flows:[11]

$$\frac{\partial \hat{f}}{\partial t} + V_i \frac{\partial \hat{f}}{\partial x_i} = \frac{1}{\rho} \frac{\partial \langle \mathscr{P} \rangle}{\partial x_i} \frac{\partial \hat{f}}{\partial V_i} + \frac{\partial}{\partial V_i} \left[\hat{f} \left\langle \frac{1}{\rho} \frac{\partial p}{\partial x_i} - \nu \frac{\partial^2 U_i}{\partial x_j \partial x_j} \middle| \mathbf{U}(\mathbf{x},t) = \mathbf{V} \right\rangle \right]. \tag{3}$$

To close Eq. (3), we consider an ensemble of fluid particles moving through the velocity field with position $\mathscr{X}(t)$ and velocity $\mathscr{U}(t)$. The exact evolution equations for these particles are[12]

$$d\mathscr{X}_i = \mathscr{U}_i dt \tag{4}$$

 1070-6631/97/9(9)/2692/12/$10.00

$$d\mathscr{U}_i = -\frac{1}{\rho}\frac{\partial\langle\mathscr{P}\rangle}{\partial x_i}dt + \nu\frac{\partial^2\langle U_i\rangle}{\partial x_j\partial x_j}dt - \frac{1}{\rho}\frac{\partial p}{\partial x_i}dt + \nu\frac{\partial^2 u_i}{\partial x_j\partial x_j}dt. \tag{5}$$

To form a closure model with these particle equations, we distinguish between known terms and unknown terms. For a pdf particle formulation, the dependent variables are the particle properties, the pdf, and everything that can be derived from the pdf. So for example the mean velocity,

$$\langle U_i\rangle = \int V_i f d\mathbf{V}, \tag{6}$$

is known, and the mean pressure is known through its solution to the Poisson equation.[11] On this basis, we see that only the last two terms on the right hand side of Eq. (5) are unknown and need to be modeled. We neglect the second term on the right hand side on the grounds that it is sufficiently small in high Reynolds number flows, and we model the unknown terms using the Simplified Langevin model[13] to give

$$d\mathscr{X}_i = \mathscr{U}_i dt, \tag{7}$$

$$d\mathscr{U}_i = -\frac{1}{\rho}\frac{\partial\langle\mathscr{P}\rangle}{\partial x_i}dt - \left(\frac{1}{2}+\frac{3}{4}C_0\right)\langle\omega\rangle(\mathscr{U}_i - \langle U_i\rangle)dt + \sqrt{C_0 k\langle\omega\rangle}\, dW_i. \tag{8}$$

Here, C_0 is a positive model constant,

$$k = \frac{1}{2}\langle u_i u_i\rangle \tag{9}$$

is the turbulent kinetic energy, and dW_i is an increment of the isotropic Wiener process $\mathbf{W}$, in which each increment is normal $(0,dt)$ and

$$dW_i\, dW_j = dt\,\delta_{ij}. \tag{10}$$

The term $\langle\omega\rangle$ is the mean characteristic turbulent frequency. In most Reynolds-stress closures, $\langle\omega\rangle$ is determined by solving an equation for the mean dissipation ϵ, and then setting

$$\langle\omega\rangle = \frac{\epsilon}{k}, \tag{11}$$

for high Reynolds number turbulence. Here, we adopt an approach more akin to Wilcox's $k-\omega$ model[14] by solving a stochastic particle equation for a property ω. The best physical interpretation for this ω is as an instantaneous turbulent frequency. Equation (11) suggests that for high Reynolds number flows, we have

$$\omega = \frac{\nu}{k}\left(\frac{\partial u_i}{\partial x_j}\frac{\partial u_i}{\partial x_j}\right). \tag{12}$$

Based upon previous formulations,[15,16] the evolution equation for ω is

$$d\omega = -C_3\langle\omega\rangle(\omega - \langle\omega\rangle)dt - S_\omega\langle\omega\rangle\omega\, dt + \sqrt{2C_3C_4\langle\omega\rangle^2\omega}\, dW', \tag{13}$$

where C_3 and C_4 are model constants and dW' is another Wiener process, independent from the one which appears in Eq. (8). The term involving S_ω accounts for generation and loss of mean turbulent frequency. For model constants $C_{\omega1}$ and $C_{\omega2}$,

$$S_\omega = C_{\omega2} - C_{\omega1}\frac{P}{\epsilon}, \tag{14}$$

where P is the production of k:

$$P = -\langle u_i u_j\rangle\frac{\partial\langle U_i\rangle}{\partial x_j}. \tag{15}$$

The constant C_4 controls the variance of the distribution of ω, and C_3 controls the extent to which ω correlates with other particle properties such as velocity. We will see in Section III that those correlations are important for the transport of $\langle\omega\rangle$ in inhomogeneous flows.

Let $f(\mathbf{V},\Omega;\mathbf{x},t)$ be the modeled Eulerian joint pdf of velocity and turbulent frequency. From the particle evolutions given in Eqs. (7), (8), and (13), this pdf evolves by

$$\frac{\partial f}{\partial t} + V_i\frac{\partial f}{\partial x_i} = \frac{\partial f}{\partial V_i}\frac{1}{\rho}\frac{\partial\langle\mathscr{P}\rangle}{\partial x_i} + \left(\frac{1}{2}+\frac{3}{4}C_0\right)\langle\omega\rangle \times\frac{\partial}{\partial V_i}[(V_i - \langle U_i\rangle)f] + \frac{1}{2}C_0 k\langle\omega\rangle\frac{\partial^2 f}{\partial V_i\partial V_i} + C_3\langle\omega\rangle\frac{\partial}{\partial\Omega}[(\Omega - \langle\omega\rangle)f] + S_\omega\langle\omega\rangle\frac{\partial}{\partial\Omega}(\Omega f) + C_3C_4\langle\omega\rangle^2\frac{\partial^2(\Omega f)}{\partial\Omega\partial\Omega}. \tag{16}$$

The major points of how this is derived are described in Refs. 17, 11, 19, and 18. The integral of Eq. (16) over Ω space provides a pdf closure for Eq. (3).

B. Relationship to Reynolds-stress closures

The relationship of the above pdf model with Reynolds-stress closures becomes apparent from the moments of Eq. (16). In general, the evolution equation for any mean quantity $\langle\phi\rangle$ is derived by multiplying Eq. (16) by Φ (the sample space variable from which ϕ is chosen) and then integrating over velocity and frequency space. Performing this calculation with velocity U_i, with the product of fluctuating velocities $u_i u_j$, and with ω, we arrive at the moment evolution equations associated with Eq. (16). This procedure is described in detail in Ref. 19. We also include an evolution equation for the correlation $\langle u_i\omega\rangle$ which appears as a transport term in the $\langle\omega\rangle$ equation, because it proves useful in Section IV where the boundary conditions are specified. For

$$\frac{\widetilde{D}(\cdot)}{Dt} = \frac{\partial(\cdot)}{\partial t} + \langle U_k\rangle\frac{\partial(\cdot)}{\partial x_k}, \tag{17}$$

these moment equations are

$$\frac{\widetilde{D}\langle U_j\rangle}{Dt} = -\frac{\partial}{\partial x_i}\langle u_i u_j\rangle - \frac{1}{\rho}\frac{\partial\langle\mathscr{P}\rangle}{\partial x_j}, \tag{18}$$

$$\frac{\tilde{D}\langle u_i u_j\rangle}{Dt} = -\frac{\partial\langle u_i u_j u_k\rangle}{\partial x_k} - \left(\langle u_i u_k\rangle \frac{\partial\langle U_j\rangle}{\partial x_k} + \langle u_j u_k\rangle \frac{\partial\langle U_i\rangle}{\partial x_k}\right) - \left(1+\frac{3}{2}C_0\right)\langle\omega\rangle\langle u_i u_j\rangle + C_0 k\langle\omega\rangle\delta_{ij}, \tag{19}$$

$$\frac{\tilde{D}\langle\omega\rangle}{Dt} = -\frac{\partial\langle u_i\omega\rangle}{\partial x_i} - S_\omega\langle\omega\rangle^2, \tag{20}$$

$$\frac{\tilde{D}\langle u_i\omega\rangle}{Dt} = -\frac{\partial}{\partial x_j}\langle u_i u_j\omega\rangle + \langle\omega\rangle\frac{\partial\langle u_i u_j\rangle}{\partial x_j} - \langle u_j\omega\rangle\frac{\partial\langle U_i\rangle}{\partial x_j} - \left(\frac{1}{2}+\frac{3}{4}C_0\right)\langle\omega\rangle\langle u_i\omega\rangle - C_3\langle\omega\rangle\langle u_i\omega\rangle - S_\omega\langle\omega\rangle \times\langle u_i\omega\rangle. \tag{21}$$

This development reproduces the Reynolds equations exactly in Eq. (18), except for the viscous term which is neglected. Moreover, it provides the Reynolds-stress equations with turbulent transport and production represented exactly, and with a model [on the second line of Eq. (19)] for the correlations of fluctuating velocity–pressure gradients and the dissipation. Substitution of

$$C_0 = \frac{2}{3}(C_1 - 1), \tag{22}$$

shows[13] that these terms are identical to Rotta's model with constant C_1.

Equation (20) describes the evolution of mean turbulent frequency. It is the analog of the more commonly used ϵ equation, with the production and dissipation of $\langle\omega\rangle$ given by the expression for S_ω in Eq. (14). Equations (7)–(9), (11), and (13)–(20) form the basic model with which the pdf wall function is developed.

III. MODELS FOR THE LOG LAYER

Wall-function boundary conditions are based on the idea that equilibrium flow conditions exist in a region of the flow close to the wall. Here, we develop two models to characterize these conditions in a pdf formulation: The first is a pdf version of the constant-stress layer,[20] which is used to describe the joint pdf of **U** and ω and to bring out how the von Kármán constant κ is related to the model constants in Eqs. (8) and (13). The second model is a linear-stress layer, which provides a more accurate representation of the Reynolds stresses in the logarithmic region. This linear-stress model is useful for the specification of the shear stress. Both models are used to provide guidance in the different aspects of pdf wall functions.

A. Constant-stress layer

The constant-stress analysis is used here to explore the properties of $f(\mathbf{V},\Omega;\mathbf{x},t)$, the joint pdf of velocity and frequency, and to calibrate the model constants for the logarithmic velocity profile. We assume that the turbulent statistics depend only on y, the mean velocity profile is logarithmic in y, the Reynolds stresses do not depend on y, the Reynolds shear stress is equal to the shear stress at the wall, production equals dissipation, and both vary inversely with the distance y. For a wide range of $k-\epsilon$ and Reynolds-stress models, these conditions can be combined to form an analytical solution to the governing equations, called the constant-stress layer solution.

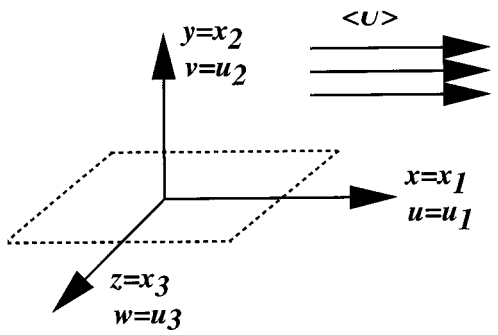

FIG. 1. Coordinate system relative to the wall and the mean flow.

For the model of Eqs. (7), (8), and (13), and for coordinates shown in Figure 1, we seek a self-similar solution to the pdf transport equation (16) which is consistent with the assumptions described above. If such a solution exists, then Eqs. (18) and (19) guarantee that the profiles of the relevant statistics are

$$\frac{\partial\langle U\rangle}{\partial y} = \frac{u_*}{\kappa y}, \tag{23}$$

$$\frac{k}{u_*^2} = \frac{3C_0+2}{2\sqrt{C_0}}, \tag{24}$$

$$\frac{\langle u^2\rangle}{u_*^2} = \frac{C_0+2}{\sqrt{C_0}}, \tag{25}$$

$$\frac{\langle v^2\rangle}{u_*^2} = \frac{\langle w^2\rangle}{u_*^2} = \sqrt{C_0}, \tag{26}$$

$$\frac{\langle uv\rangle}{u_*^2} = -1, \tag{27}$$

$$\epsilon = \frac{u_*^3}{\kappa y}, \tag{28}$$

$$\langle\omega\rangle = \frac{2\sqrt{C_0}}{3C_0+2}\frac{u_*}{\kappa y}, \tag{29}$$

where

$$u_* = \sqrt{\frac{\tau_w}{\rho}} \tag{30}$$

is the friction velocity and τ_w is the shear stress at the wall. The constant κ which appears in the expression for the velocity gradient and the mean frequency is the von Kármán constant for the logarithmic layer of the mean velocity profile. In this constant-stress layer solution, the value of κ is controlled by the balance of terms in Eq. (20).

The self-similar solution to Eq. (16) is determined using a Monte Carlo method, similar to the approach which ap-

pears in Ref. 21. We find a similarity solution by transforming the model of Eqs. (7), (8), and (13) to one which admits such a solution. This occurs in four steps: First we define the relevant similarity variables and write down their particle evolution equations. Second, we show the associated pdf evolution equation. Third, we assume self-similarity, plus the constant-stress layer conditions to find a simplified pdf equation. And fourth, we write particle equations associated with this simplified pdf equation; these particle equations form the basis for a zero-dimensional Monte Carlo simulation.

Let

$$\widetilde{u}_i(t)=\frac{\mathscr{U}_i(t)-\langle U_i\rangle[\mathscr{X}(t),t]}{u_*}, \tag{31}$$

$$\widetilde{\omega}(t)=\frac{\omega(t)\mathscr{X}_2(t)}{u_*}, \tag{32}$$

be the particle fluctuating velocities and turbulent frequency, respectively, normalized by the friction velocity. The associated sample-space variables are $\widetilde{v}_i$ and $\widetilde{\Omega}$. We seek a solution for $g(\widetilde{\mathbf{v}},\widetilde{\Omega};\mathbf{x},t)$, the joint pdf of $\widetilde{\mathbf{u}}$ and $\widetilde{\omega}$; which is independent of $\mathbf{x}$ and t. Substituting Eqs. (31)–(32) into the model of Eqs. (7), (8), and (13), we find new particle equations, simplified for statistically one-dimensional flow:

$$d\mathscr{X}_2=\widetilde{u}_2u_*dt, \tag{33}$$

$$d\widetilde{u}_i=u_*\frac{\partial\langle\widetilde{u}_i\widetilde{u}_2\rangle}{\partial x_2}dt-\frac{\partial\langle U_i\rangle}{\partial x_2}\widetilde{u}_2dt-\left(\frac{3}{4}C_0+\frac{1}{2}\right)\langle\omega\rangle\widetilde{u}_idt+\sqrt{C_0\widetilde{k}\langle\omega\rangle}\,dW_i, \tag{34}$$

$$d\widetilde{\omega}=\frac{\widetilde{\omega}}{\mathscr{X}_2}\widetilde{u}_2u_*dt-C_3\langle\omega\rangle\left(\widetilde{\omega}-\frac{\mathscr{X}_2\langle\omega\rangle}{u_*}\right)dt-S_\omega\langle\omega\rangle\widetilde{\omega}\,dt+\sqrt{2C_3C_4\langle\omega\rangle^2\widetilde{\omega}\frac{\mathscr{X}_2}{u_*}}\,dW'. \tag{35}$$

The associated pdf evolution equation for g is

$$\frac{\partial g}{\partial t}+u_*\widetilde{v}_2\frac{\partial g}{\partial x_2}=\frac{\partial\langle U_i\rangle}{\partial x_2}\frac{\partial(g\widetilde{v}_2)}{\partial\widetilde{v}_i}-u_*\frac{\partial\langle\widetilde{u}_i\widetilde{u}_2\rangle}{\partial x_2}\frac{\partial g}{\partial\widetilde{v}_i}+\left(\frac{3}{4}C_0+\frac{1}{2}\right)\langle\omega\rangle\frac{\partial(\widetilde{v}_ig)}{\partial\widetilde{v}_i}+\frac{1}{2}C_0\widetilde{k}\langle\omega\rangle\frac{\partial^2g}{\partial\widetilde{v}_i\partial\widetilde{v}_i}+C_3\langle\omega\rangle\frac{\partial}{\partial\widetilde{\Omega}}\left[\left(\widetilde{\Omega}-\frac{x_2\langle\omega\rangle}{u_*}\right)g\right]+\left(S_\omega\langle\omega\rangle-\frac{\widetilde{v}_2u_*}{x_2}\right)\frac{\partial(\widetilde{\Omega}g)}{\partial\widetilde{\Omega}}+C_3C_4\langle\omega\rangle^2\frac{x_2}{u_*}\frac{\partial^2(\widetilde{\Omega}g)}{\partial\widetilde{\Omega}^2}. \tag{36}$$

The self-similar pdf equation is obtained by noting that

$$\langle\widetilde{\omega}\rangle=\frac{x_2\langle\omega\rangle}{u_*}, \tag{37}$$

and by assuming that all dependence of g on time and on space vanishes:

$$0=\frac{x_2}{u_*}\frac{\partial\langle U_i\rangle}{\partial x_2}\widetilde{v}_2\frac{\partial g}{\partial\widetilde{v}_i}+\left(\frac{3}{4}C_0+\frac{1}{2}\right)\langle\widetilde{\omega}\rangle\frac{\partial(\widetilde{v}_ig)}{\partial\widetilde{v}_i}+\frac{1}{2}C_0\widetilde{k}\langle\widetilde{\omega}\rangle\frac{\partial^2g}{\partial\widetilde{v}_i\partial\widetilde{v}_i}+(S_\omega\langle\widetilde{\omega}\rangle-\widetilde{v}_2)\frac{\partial(\widetilde{\Omega}g)}{\partial\widetilde{\Omega}}+C_3\langle\widetilde{\omega}\rangle\frac{\partial}{\partial\widetilde{\Omega}}[(\widetilde{\Omega}-\langle\widetilde{\omega}\rangle)g]+C_3C_4\langle\widetilde{\omega}\rangle^2\frac{\partial^2(\widetilde{\Omega}g)}{\partial\widetilde{\Omega}^2}. \tag{38}$$

This is solved by a Monte Carlo method, using just the stationary solution to these particle equations for $\widetilde{\mathbf{u}}$ and $\widetilde{\omega}$:

$$d\widetilde{u}_i=-\frac{x_2}{u_*}\frac{\partial\langle U_1\rangle}{\partial x_2}\widetilde{u}_2\delta_{i1}dt-\left(\frac{3}{4}C_0+\frac{1}{2}\right)\langle\widetilde{\omega}\rangle\widetilde{u}_idt+\sqrt{C_0\widetilde{k}\langle\widetilde{\omega}\rangle}\,dW_i, \tag{39}$$

$$d\widetilde{\omega}=\widetilde{\omega}\widetilde{u}_2dt-C_3\langle\widetilde{\omega}\rangle(\widetilde{\omega}-\langle\widetilde{\omega}\rangle)dt-S_\omega\langle\widetilde{\omega}\rangle\widetilde{\omega}\,dt+\sqrt{2C_3C_4\langle\widetilde{\omega}\rangle^2\widetilde{\omega}}\,dW. \tag{40}$$

Eq. (39) is identical for $\widetilde{u}_2$ and $\widetilde{u}_3$. It should be noted that particle equations (39) and (40) are not consistent with Eqs. (33) through (35), and that one set cannot be derived from the other. The relevant feature here is that Eqs. (39) and (40) can be used to solve the pdf equation (36) for this case in which g has no dependence on space and time. All of the model constants of Eqs. (39) and (40) except for C_3 are assigned standard values:[16,21,15]

$$C_0=3.5, \tag{41}$$

$$C_4=0.25, \tag{42}$$

$$S_\omega=C_{\omega2}-C_{\omega1}=0.46. \tag{43}$$

For a given set of model constants, there is only one value of $(x_2/u_*)(\partial\langle U_1\rangle/\partial x_2)$ which permits a self-similar solution. To be consistent with the logarithmic mean velocity profile, we impose the condition that

$$\frac{x_2}{u_*}\frac{\partial\langle U_1\rangle}{\partial x_2}=\frac{1}{\kappa}=\frac{1}{0.41}, \tag{44}$$

and use the Monte Carlo simulation[22] to determine which value of C_3 makes that value of κ possible. This procedure gives a value of $C_3=5.0$.

Probability density functions are estimated from the simulation results by dividing the particle properties in question into 40 bins and taking a normalized sum of particles which fall into each bin. The marginal pdfs of $\widetilde{u}_1$ and $\widetilde{u}_2$ are shown in Figure 2, and the marginal pdf of $\widetilde{\omega}$ is shown in

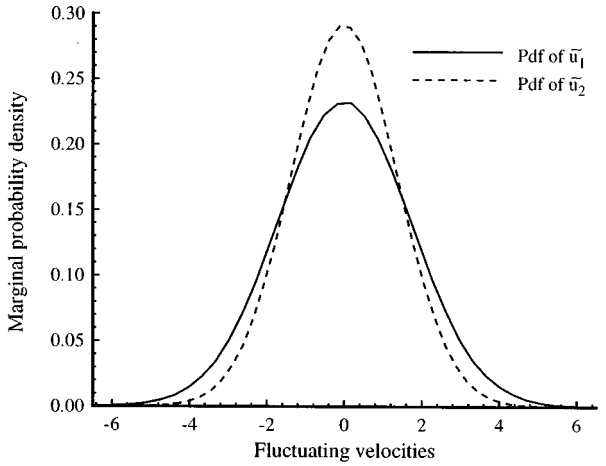

FIG. 2. Marginal pdfs of $\widetilde{u}_1$ and $\widetilde{u}_2$ for the self-similar constant-stress layer.

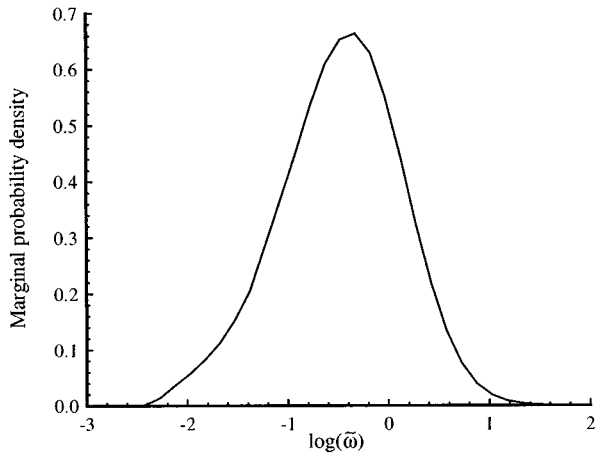

FIG. 4. Marginal pdf of $\log(\widetilde{\omega})$ for the self-similar constant-stress layer.

Figure 3. (The pdf of $\widetilde{u}_3$ is identical to that of $\widetilde{u}_2$, and not shown.) The pdfs of velocity are clearly Gaussian, both with skewness of magnitude less than 0.02, and flatness within 1% of the Gaussian flatness of 3. The variances of $\widetilde{u}_1$ and $\widetilde{u}_2$ are within 1% of the values of 2.94 and 1.87, respectively, which Eqs. (25) and (26) stipulate. These velocity results are not surprising since the Langevin equation (39) admits joint normal solutions. The distribution of $\widetilde{\omega}$ is strongly skewed with a skewness of 2.1; this is also a reasonable result because Eq. (40) is similar to the ω model of Ref. 15 which admits a Γ distribution as a solution. The mean of $\widetilde{\omega}$ is also within 1% of its theoretical value of 0.73, taken from Eqs. (29) and (37).

Experimental and DNS results of the velocity distribution in the log layer for various near-wall flows are described in Refs. 23, 24. Gaussian behavior is observed in the spanwise velocity, but there are departures in the streamwise and wall–normal components: In the log layer, skewness of $\langle u^2 \rangle$ varies from approximately -0.6 to 0, and skewness of $\langle v^2 \rangle$ varies between 0 and 0.3. In isotropic turbulence,[25] log-normal behavior of dissipation (and hence of turbulent frequency) is observed. The marginal pdf of $\log(\widetilde{\omega})$ is shown in Figure 4. While this still has a skewness of -0.23, the behavior of $\log(\widetilde{\omega})$ is considerably closer to Gaussian than that of $\widetilde{\omega}$.

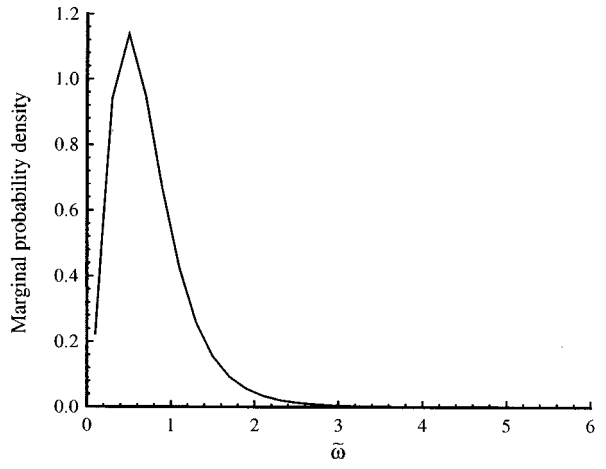

FIG. 3. Marginal pdf of $\widetilde{\omega}$ for the self-similar constant-stress layer.

For the purposes of pdf wall functions, the important priorities are to have a plausible, robust joint pdf of velocity and frequency, accurate reproduction of the ratio of turbulent kinetic energy to shear stress, and of the logarithmic velocity profile. Accordingly, a joint-normal pdf of **U** and $\log(\omega)$ is used to specify boundary conditions on particles. The model constant $C_0 = 3.5$ sets the ratio $k/-\langle u_1 u_2 \rangle = 3.3$ through Eqs. (24) and (27).

In a constant-stress wall layer, the shape of the logarithmic mean velocity profile is characterized by the von Kármán constant, κ. In the more traditional $k-\epsilon$ and Reynolds-stress models, the value of κ is set to the experimentally found value of $\kappa = 0.41$ through the balance of terms in the ϵ equation. The model constant σ_ϵ controls the value of κ by adjusting the role of the transport term relative to the other terms.[20] With pdf models, we calibrate κ by adjusting the transport term in Eq. (20), relative to the source and sink terms which appear there. Unlike in a Reynolds-stress closure, the transport of $\langle \omega \rangle$ is not closed in the moment equation, only in the pdf evolution equation, Eq. (16). And its role in the balance of terms in Eq. (20) must be controlled elsewhere, namely in the adjustment of C_3 in Eq. (13). Previous values of C_3 ranging between $C_3 = 1.0$ and 2.0 have been used[16,21,15] in the model for ω, based on DNS results for isotropic turbulence. In the current context, we choose C_3 for its role in an inherently inhomogeneous (and hence anisotropic) process, the transport of $\langle \omega \rangle$. The constant C_3 adjusts the extent to which ω correlates with particle position, and hence with particle velocity. Figure 5 shows this correlation between ω and particle velocity in the constant-stress layer. As C_3 increases, $\langle v\,\omega \rangle$ decreases, and the resulting balance of terms in Eq. (20) makes κ increase. Different combinations of C_3 and κ which admit self-similar solutions of Eq. (38) are shown in Figure 6. For the constant-stress layer, the logarithmic profile with $\kappa = 0.41$ occurs in this model by setting $C_3 = 5.0$.

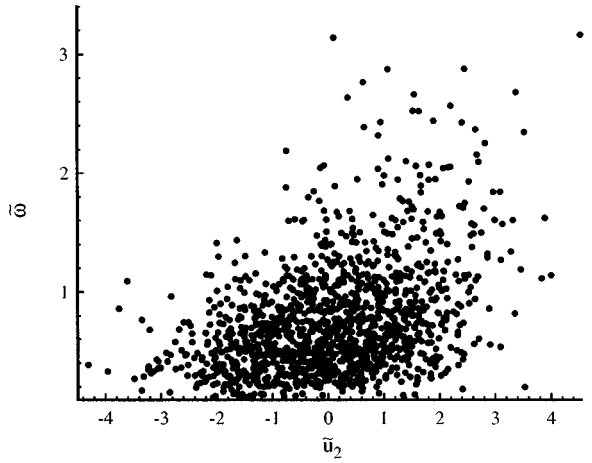

FIG. 5. Scatter of $\widetilde{u_2}$ and $\widetilde{\omega}$ for the self-similar constant-stress layer.

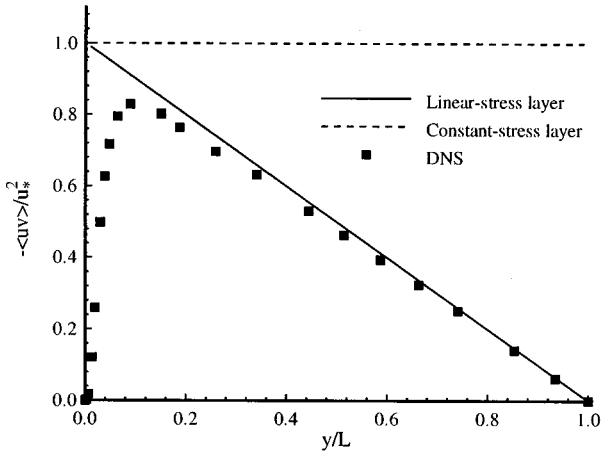

FIG. 7. Reynolds shear stress for fully-developed channel flow: comparison of constant-stress layer, linear-stress layer, and DNS.

B. Linear-stress layer

The purpose of the linear-stress layer is to provide guidance for the statistical aspects of the boundary conditions for flows at moderate Reynolds numbers. While most wall functions are formulated with the constant-stress argument in mind, that argument is only valid in the limit as $Re \to \infty$. Consider the fully-developed channel flow of Mansour, with halfwidth L and a moderate $Re_\tau = u_* L/\nu = 395$. Figure 7 shows the Reynolds shear stress of the DNS results[26] and of the constant-stress profile given by Eq. (27), plus the linear-stress profile described below. Accurate representation of the shear stress is a central priority of the wall functions developed here; it is clear from Figure 7 that the constant-stress layer is an inadequate model from which to determine the shear stress. A description of the flow is needed which more accurately represents the turbulent stresses, but which also preserves the results of the constant-stress analysis concerning the ratio $k/\langle uv\rangle$ and the calibration of κ in the log layer.

The linear-stress layer is an approximation of a solution to the governing moment equations (18) through (21), with less cavalier assumptions about the nature of the flow than those of the constant-stress argument. Based on well-established observations of equilibrium wall-bounded flows,[8–10] we assume that the flow is homogeneous in all but the wall–normal direction, and that the streamwise pressure gradient is independent of y, plus the following:

$$\frac{\partial \langle U\rangle}{\partial y} = \frac{u_c}{\kappa y}, \tag{45}$$

$$P = \epsilon, \tag{46}$$

$$\frac{k}{-\langle uv\rangle} = \text{const}, \tag{47}$$

where u_c is a characteristic turbulent velocity scale. The issues involved in choosing u_c are discussed in Ref. 27. It can either be set to the friction velocity u_*, or it can be based on the local shear stress and set to $\sqrt{-\langle uv\rangle}$. We use the Huang and Bradshaw choice of

$$u_c = u_*, \tag{48}$$

on grounds similar to theirs: Use of the local shear stress implies an approximately logarithmic velocity profile in which κ depends on the pressure gradient. The choice of $u_c = u_*$ preserves the relative insensitivity of κ to $\partial\langle \mathscr{P}\rangle/\partial x$ which is generally observed. The profiles of k and $\langle uv\rangle$ differ here from those of the constant-stress layer, but their ratio is specified to be the same. Using Eqs. (24) and (27) we have

$$\frac{k}{-\langle uv\rangle} = \frac{3C_0 + 2}{2\sqrt{C_0}}. \tag{49}$$

To simplify the analysis, $k-\epsilon$ notation is used: For $C_0 = 3.5$ and

$$C_\mu = \frac{4C_0}{(3C_0+2)^2} = 0.09, \tag{50}$$

we have

$$\frac{k}{-\langle u_1 u_2\rangle} = \frac{1}{\sqrt{C_\mu}} = 3.33. \tag{51}$$

Under the above assumptions, profiles of $\langle uv\rangle$, k, ϵ, and $\langle \omega\rangle$ are determined with an argument similar to the development for turbulent viscosity and mixing length of Ref. 27.

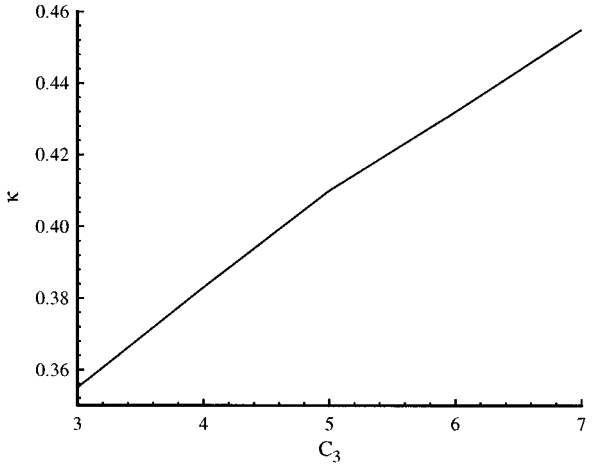

FIG. 6. Model κ vs constant C_3 for the self-similar constant-stress layer.

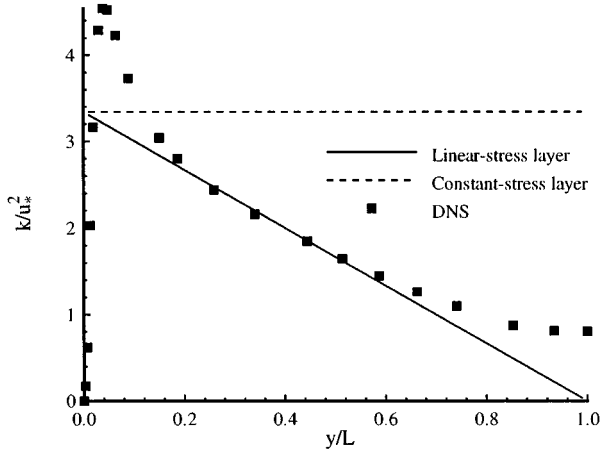

FIG. 8. Turbulent kinetic energy for fully-developed channel flow: comparison of constant-stress layer, linear-stress layer, and DNS.

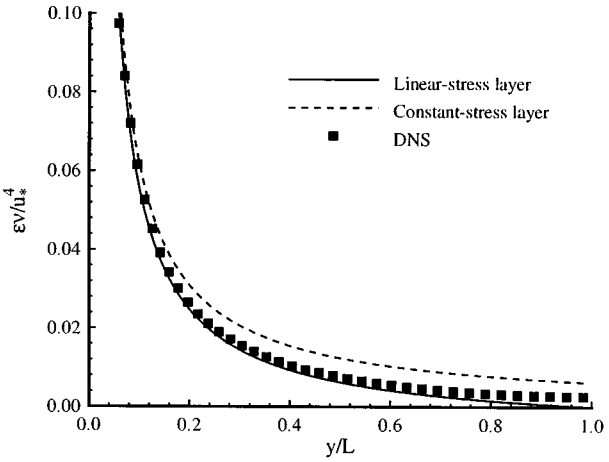

FIG. 9. Dissipation for fully-developed channel flow: comparison of constant-stress layer, linear-stress layer, and DNS.

Let L_P be a length scale to characterize the effect of the pressure gradient relative to the wall shear stress. For the coordinate system of Figure 1,

$$L_P = \frac{-\rho u_*^2}{\frac{\partial \langle \mathscr{P} \rangle}{\partial x}}. \tag{52}$$

For fully-developed channel flow, L_P is equal to the channel halfwidth. The profile for the Reynolds shear stress is obtained by integrating Eq. (18) from the wall to y:

$$\frac{\langle u_1 u_2 \rangle}{u_*^2} = \frac{y}{L_P} - 1. \tag{53}$$

The profile of k follows from Eqs. (51) and (53):

$$\frac{k}{u_*^2} = \frac{1 - \frac{y}{L_P}}{\sqrt{C_\mu}}. \tag{54}$$

The profile of dissipation comes from Eqs. (45), (46), and (53):

$$\epsilon = \frac{u_*^3 \left(1 - \frac{y}{L_P} \right)}{\kappa y}. \tag{55}$$

And from Eqs. (11), (50), and (55), it is clear that the profile of $\langle \omega \rangle$ is identical to its profile in the constant-stress layer, given by Eq. (29). The linear-stress layer profiles which differ from their constant-stress layer counterparts are all Reynolds-stress components and ϵ; they have an additional term which reflects a linear dependence on y and on the pressure gradient. The constant-stress layer can be construed as a limiting case of the linear-stress layer, in which $\partial \langle \mathscr{P} \rangle / \partial x \to 0$, $L_P \to \infty$, and all y dependence of the Reynolds stresses vanishes. The linear-stress profiles of k, $-\langle uv \rangle$, and ϵ are shown together with DNS data for fully-developed channel flow in Figures 7, 8, and 9. For this flow, the velocity profile is logarithmic over the interval $0.1 < y_p < 0.4$. The linear-stress layer is clearly the better model on which to base a specification of shear stress in the log layer for moderate Reynolds numbers. This improvement over the constant-stress layer does not reflect a Reynolds number dependence of the flow *per se*. It only reflects the fact that as Re decreases, the near-wall peak in $-\langle uv \rangle$ also decreases. For these cases, the constant-stress approximation,

$$\frac{-\langle uv \rangle}{u_*^2} = 1, \tag{56}$$

becomes steadily worse, whereas the linear-stress profile remains a good approximation.

But do these profiles satisfy the governing moment equations? It is straightforward to show that the linear-stress profiles are solutions to Eqs. (18) and (19) if the turbulent transport terms are neglected. The $\langle \omega \rangle$ equation is a little more involved. Under the assumptions of the linear-stress layer, Eq. (20) becomes

$$-\frac{\partial \langle v \omega \rangle}{\partial y} - S_\omega \langle \omega \rangle^2 = 0. \tag{57}$$

The linear-stress profiles suggest using the variables

$$\widetilde{u}_i' = \frac{u_i'}{u_* \sqrt{1 - \frac{y}{L_P}}}, \tag{58}$$

$$\widetilde{k} = \frac{k}{u_*^2 \left(1 - \frac{y}{L_P} \right)}, \tag{59}$$

$$\widetilde{\omega} = \frac{\omega y}{u_*}, \tag{60}$$

to seek an equation in which the dependence on y vanishes. Transforming Eq. (57) with the above variables, we have

$$\langle \tilde{u}_2' \tilde{\omega} \rangle \left[\frac{1 - \frac{1}{2}\frac{y}{L_P}}{\sqrt{1 - \frac{y}{L_P}}} \right] - S_\omega \langle \tilde{\omega} \rangle^2 = 0. \tag{61}$$

The term in square brackets embodies the y dependence of the transformed $\langle \omega \rangle$ equation. As $y \to 0$, that term approaches 1, and the linear-stress profiles become an approximate self-similar solution to the Reynolds-stress and $\langle \omega \rangle$ equations. In that limit, the $\langle \tilde{\omega} \rangle$ equation is identical to the one which appears in the constant-stress analysis. This can be verified by multiplying Eq. (38) by $\tilde{\Omega}$ and integrating over all $\tilde{\mathbf{v}}$ and $\tilde{\Omega}$. So the basis on which κ is determined with the constant-stress analysis is also valid in the linear-stress analysis. As y increases from 0, the term in square brackets departs from unity and its dependence on y increases. For values of y above a threshold, the system of equations (18) through (20) departs significantly from self-similarity, and the velocity profile is no longer logarithmic. This threshold depends on the outer flow characteristics embodied in the length scale L_P.

The constant-stress and linear-stress analyses form the basis of the pdf wall-function boundary conditions. The constant-stress layer is a self-similar solution to the pdf transport equation (3). In Section IV, this layer is used to guide the specification of κ for the logarithmic velocity profile, and to provide particle boundary conditions which ensure that the joint pdf of $\mathbf{U}$ and $\log \omega$ is approximately normal. The linear-stress layer is an approximate solution to the first- and second-moment equations associated with Eq. (16), and it is used in Section IV to ensure accurate specification of the shear stress at the boundary.

IV. BOUNDARY CONDITIONS

The pdf wall function described in this section provides a wall boundary treatment in which the joint pdf of velocity and frequency has the characteristics of the constant-stress layer, but has the first- and second-order velocity statistics of the linear-stress layer. It must also meet more stringent stability requirements than those of the moment-closure models. This is because the coefficients which appear in the boundary conditions are subject to statistical fluctuations, and the formulation needs to be stable with respect to these fluctuations.

Traditional wall functions involve conditions on statistics: mean velocity, Reynolds stresses, mean dissipation. The problem of wall functions for the pdf method is, how do we specify a condition on *particles* to impose a desired condition on a statistic? Following the analysis of Ref. 28, consider a plane parallel to the wall at the location y_p where the boundary condition is to be imposed. This location should correspond to a value greater than $y^+ = 30$, but sufficiently close to the wall to be in the inertial sublayer for an equilibrium flow. Figure 10 shows how the boundary condition on particles preserves mass conservation and impermeability in the mean: For every particle with properties $\underline{\phi}_I$ that leaves the flow domain by crossing the plane at y_p, another particle

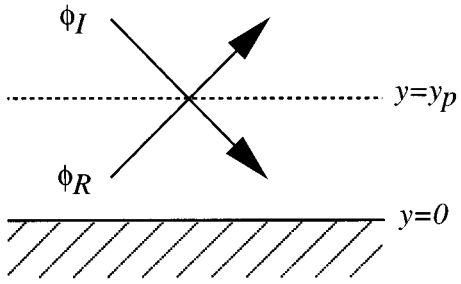

FIG. 10. Particles reflecting through the plane at y_p.

with properties $\underline{\phi}_R$ enters the domain at the same location. The subscripts here are I for incident and R for reflected. Then the mean value of any function $h(\underline{\phi})$, at the plane is

$$\langle h(\underline{\phi}) \rangle_p = \frac{1}{2} [\langle h(\underline{\phi}_I) \rangle + \langle h(\underline{\phi}_R) \rangle]. \tag{62}$$

To impose a desired value of the statistic $\langle h(\underline{\phi}) \rangle_p$, we specify the reflected particle properties $\underline{\phi}_R$ so that Eq. (62) is satisfied for each pairwise exchange of particles through the plane at the location y_p. This ensures that Eq. (62) is also satisfied in the mean.

A. Conditions on velocity

Let $\mathscr{U}$ and $\mathscr{V}$ be the streamwise and wall–normal particle velocities, respectively. The statistics to be specified are the wall–normal mean velocity $\langle V \rangle_p$, and the shear stress $\langle uv \rangle_p$. We use particle boundary conditions which preserve Gaussianity of the velocities found in the constant-stress pdf solution. The condition on $\langle V \rangle_p$ is straightforward: To impose the statistical condition that

$$\langle V \rangle_p = 0, \tag{63}$$

we impose Eq. (62) on each pair of particles leaving and entering the domain. This requires that

$$\mathscr{V}_R = -\mathscr{V}_I. \tag{64}$$

It is clear that this condition leaves that Gaussian shape of the pdf of velocity unchanged. A useful result which follows from this specification together with Eq. (62) is that

$$\langle v^2 \rangle_p = \langle \mathscr{V}_I^2 \rangle. \tag{65}$$

Next, we specify a condition on the reflected streamwise particle velocity $\mathscr{U}_R$ to impose the desired shear stress. We set

$$\mathscr{U}_R = \mathscr{U}_I + \alpha \mathscr{V}_I, \tag{66}$$

where α is to be determined by the specification of $\langle uv \rangle_p$. For the joint-normal velocity components found in the constant-stress layer, this condition preserves the shape of the pdf. To see the relationship between α and $\langle uv \rangle_p$, we substitute Eqs. (65) and (66) into Eq. (62) with $h = \mathscr{U}\mathscr{V}$ to find that

$$\alpha = \frac{-2\langle uv \rangle_p}{\langle v^2 \rangle_p}. \tag{67}$$

The argument from Eq. (62) to Eq. (67) is reported for the first time here, although it has been previously derived[28] and incorporated into the pdf method.[7] Given Eq. (67), the question then becomes, how do we specify $\langle uv\rangle_p$?

The shear stress is a central issue for conventional wall functions as well as pdf wall functions. The condition presented here differs from conventional wall functions in two respects: First we base the condition on the linear-stress profiles rather than the constant stress ones (where the profiles differ from one another) in an effort to better accommodate flows at moderate Reynolds numbers. And second, we ensure that the condition is stable with respect to its parameters, so that convergence of the pdf solutions is forgiving to statistical fluctuations of the relevant terms at the boundaries.

Let $\hat{u}$ be a velocity scale to characterize the turbulence intensity in the vicinity of y_p. We define $\hat{u}$ to be based on the turbulent kinetic energy, so that it equals the local shear velocity (i.e., $\sqrt{|\langle uv\rangle|}$) under equilibrium conditions. Equation (51) shows that this is arranged by setting

$$\hat{u}=C_\mu^{1/4}k^{1/2}. \tag{68}$$

For equilibrium conditions, the linear-stress layer distinguishes between $\hat{u}$ and u_*: u_* is constant throughout the layer, whereas $\hat{u}$ changes with y through the dependence of k on the pressure gradient term which appears in Eq. (54). Let U_e be the magnitude of the equilibrium value of the mean velocity at y_p. Based on the logarithmic profile of Eq. (45), we have

$$U_e=\frac{u_*}{\kappa}\log\left[E\frac{y_p u_*}{\nu}\right], \tag{69}$$

with the surface roughness parameter $E=8.5$ for a smooth wall. To calculate the friction velocity from the local statistics, we set

$$u_*=\sqrt{\hat{u}_p^2+\gamma_\tau\left|\frac{y_p}{\rho}\frac{\partial\langle\mathscr{P}\rangle}{\partial x}\right|}=\sqrt{\sqrt{C_\mu}k_p+\gamma_\tau\left|\frac{y_p}{\rho}\frac{\partial\langle\mathscr{P}\rangle}{\partial x}\right|}, \tag{70}$$

where

$$\gamma_\tau=\max\left[0,\operatorname{sign}\left(\langle uv\rangle\frac{\partial\langle\mathscr{P}\rangle}{\partial x}\right)\right], \tag{71}$$

and $\langle uv\rangle$ is the shear stress taken from the previous time step. The idea is that for equilibrium flows, $\langle uv\rangle$ and $\partial\langle\mathscr{P}\rangle/\partial x$ have the same sign, which makes $\gamma_\tau=1$. In this case, Eq. (70) is equivalent to the mean velocity equation (18) applied to the layer between the wall and y_p. In some non-equilibrium conditions such as separation and reattachment, $\langle uv\rangle$ and $\partial\langle\mathscr{P}\rangle/\partial x$ can have opposite signs. In such cases the physical argument behind the wall function no longer applies, and it is more important to ensure a robust boundary condition than it is to impose the physically based equation (18). So Eq. (71) makes $\gamma_\tau=0$, and Eq. (70) is reduced to setting $u_*=\hat{u}$. The specification for the boundary condition on shear stress is

$$\tau_p=-\langle u_1u_2\rangle_p=\hat{u}_p^2\frac{\langle U\rangle_p|\langle U\rangle_p|}{U_e^2}. \tag{72}$$

This amounts to setting

$$\alpha=\frac{2\hat{u}_p^2\langle U\rangle_p|\langle U\rangle_p|}{\langle v^2\rangle_p U_e^2}. \tag{73}$$

Under equilibrium conditions, $\langle U\rangle_p=U_e$ so this condition reduces to imposing the equilibrium shear stress, with the mean velocity taking on its value in the logarithmic profile. Because of the statistical fluctuations inherent in pdf Monte Carlo methods, it is important to check the stability of Eq. (72). For a small departure of $\langle U\rangle_p$ or of $\hat{u}_p$ from equilibrium, we find from Eqs. (69) through (72) that

$$\frac{\delta\tau_p}{\tau_p}=2\frac{\delta\langle U\rangle_p}{\langle U\rangle_p}+2\left[\left|\frac{y_p}{\rho u_*^2}\frac{\partial\langle\mathscr{P}\rangle}{\partial x}\right|-\frac{\hat{u}_p^2}{\kappa u_* U_e}\right]\frac{\delta\hat{u}_p}{\hat{u}_p}. \tag{74}$$

For an adequate neighborhood of flow conditions close to equilibrium [i.e., those in which the term in the square brackets of Eq. (74) is negative] this boundary condition produces a stable response of τ to perturbations in both $\langle U\rangle_p$ and $\hat{u}_p$. The complete boundary condition on particle velocities is given by Eqs. (64) and (66) through (72).

B. Condition on turbulent frequency

For the boundary condition on turbulent frequency, we seek a consistency condition which imposes the linear-stress layer profile for equilibrium conditions, and which preserves the approximate Gaussianity of the distribution of $\log(\omega)$. We know from Eq. (20) that the correlation $\langle v\omega\rangle$ is important because it provides transport of $\langle\omega\rangle$ into the domain from the near-wall region. It is plausible to construct a particle condition on ω which controls this correlation, just as Eq. (66) controls the correlation of u and v. Assuming from the constant-stress analysis that the log of ω is approximately Gaussian, we preserve the shape of the pdf by writing

$$\log\omega_R=\log\omega_I+\beta\frac{\mathscr{T}_I}{y_p\langle\omega\rangle}, \tag{75}$$

$$\omega_R=e^{\beta[\mathscr{T}_I/y_p\langle\omega\rangle]}\omega_I. \tag{76}$$

The next task is to decide what sort of statistical condition should be imposed to specify β. For the case of velocities, the calculation leading to Eq. (67) makes it clear that the shear stress $\langle uv\rangle_p$ is a natural quantity for the boundary condition. For the case with Eq. (76), the following calculation shows that the natural statistic on which to impose the boundary condition is

$$\frac{\langle\omega\rangle_p\langle\omega v\rangle_p}{\langle\omega v^2\rangle_p}. \tag{77}$$

Expanding the exponential term of Eq. (76) in a Taylor series, we have

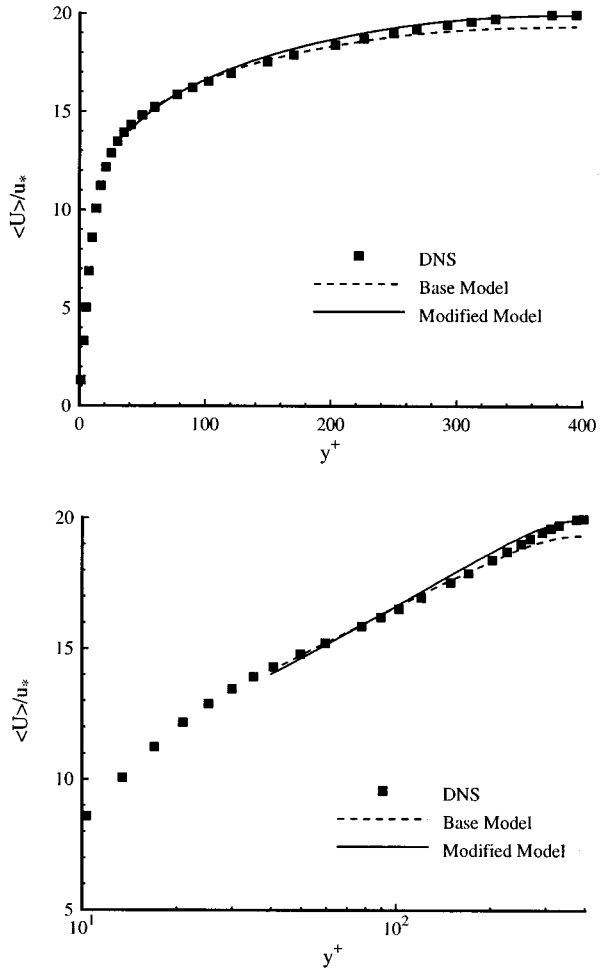

FIG. 11. Mean velocity for fully-developed channel flow: comparison of models with wall functions (lines) with DNS data (symbols).

$$\omega_R = \left[1 + \frac{\beta \mathscr{T}_I}{y_p \langle \omega \rangle_p} + \frac{1}{2}\left(\frac{\beta \mathscr{T}_I}{y_p \langle \omega \rangle_p}\right)^2 + \frac{1}{6}\left(\frac{\beta \mathscr{T}_I}{y_p \langle \omega \rangle_p}\right)^3 + \ldots\right]\omega_I. \tag{78}$$

Knowing that we can derive an expression involving $\langle \omega v \rangle$ and $\langle \omega v^2 \rangle$ from Eq. (21), we compute these moments at y_p using Eq. (78) in Eq. (62) with $h = \omega \mathscr{T}$ and with $h = \omega \mathscr{T}^2$:

$$\langle \omega v \rangle_p = -\frac{1}{2}\frac{\beta}{y_p \langle \omega \rangle_p}\langle \omega_I \mathscr{T}_I^2 \rangle - \frac{1}{4}\left(\frac{\beta}{y_p \langle \omega \rangle_p}\right)^2 \langle \omega_I \mathscr{T}_I^3 \rangle - \frac{1}{12}\left(\frac{\beta}{y_p \langle \omega \rangle_p}\right)^3 \langle \omega_I \mathscr{T}_I^4 \rangle + \ldots, \tag{79}$$

$$\langle \omega v^2 \rangle_p = \langle \omega_I \mathscr{T}_I^2 \rangle + \frac{1}{2}\frac{\beta}{y_p \langle \omega \rangle_p}\langle \omega_I \mathscr{T}_I^3 \rangle + \frac{1}{4}\left(\frac{\beta}{y_p \langle \omega \rangle_p}\right)^2 \langle \omega_I \mathscr{T}_I^4 \rangle + \ldots. \tag{80}$$

Combining these, we find that

$$\beta = \frac{-2 y_p \langle \omega \rangle_p \langle \omega v \rangle_p}{\langle \omega v^2 \rangle_p} + O(\beta^3). \tag{81}$$

This result is analogous to Eq. (67); it allows us to connect the particle condition of Eq. (76) to a statistical condition involving the moments of ω and v.

The task now is to make the appropriate specification of β. The expression in Eq. (81) is determined with the equation for $\langle \omega v \rangle$, Eq. (21). If we invoke the linear-stress layer assumptions then for $y_p << L_P$, Eq. (21) becomes

$$\langle \omega v^2 \rangle_p - \left(\frac{3}{4}C_0 + \frac{1}{2} + C_3 + C_{\omega 2} - C_{\omega 1}\right)\langle \omega \rangle_p \langle \omega v \rangle_p y_p = 0. \tag{82}$$

Using this result in Eq. (81),

$$\beta = \frac{-2}{\left(\frac{3}{4}C_0 + \frac{1}{2} + C_3 + C_{\omega 2} - C_{\omega 1}\right)}. \tag{83}$$

This specification (in conjunction with the fact that the ratio $\mathscr{T}/y_p$ is negative) gives Eq. (76) a stable response to perturbations in $\langle \omega \rangle$. The condition on ω is now complete; its reflected particle value is determined by Eqs. (76) and (83). It is a drawback of this condition that it depends on the model used for velocity and ω. But the method works for any model; it is a matter of deriving the equation for the correlation $\langle \omega v \rangle$ under what amounts to constant-stress layer conditions to find the correct specification of β.

To summarize, the particle wall-function boundary conditions for the basic model given by Eqs. (7), (8), and (13) follow:

$$\mathscr{T}_R = -\mathscr{T}_I, \tag{84}$$

$$\mathscr{U}_R = \mathscr{U}_I + \alpha \mathscr{T}_I, \tag{85}$$

$$\omega_R = e^{\beta[\mathscr{T}_I / y_p \langle \omega \rangle]}\omega_I, \tag{86}$$

with α given by Eqs. (67) through (72), and β given by Eq. (83). For a general model, the specification is the same, except that Eq. (21) must be rederived to determine β.

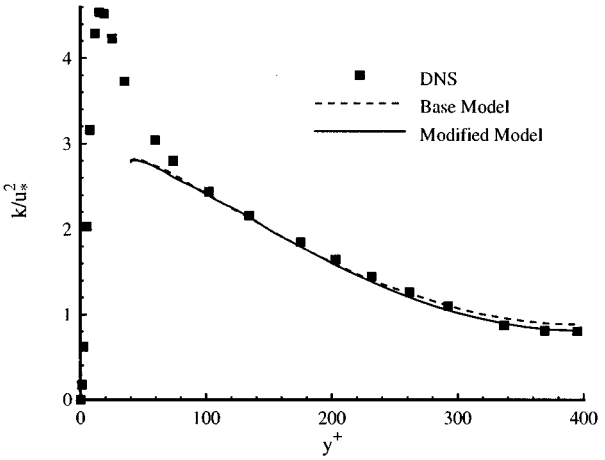

FIG. 12. Turbulent kinetic energy for fully-developed channel flow: comparison of models with wall functions (lines) with DNS data (symbols).

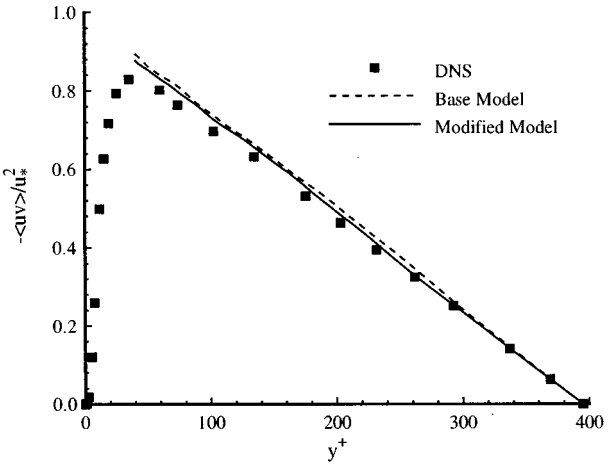

FIG. 13. Reynolds shear stress for fully-developed channel flow: comparison of models with wall functions (lines) with DNS data (symbols).

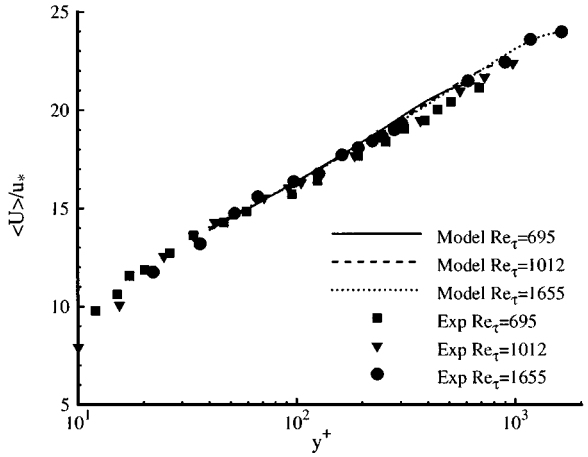

FIG. 15. Mean velocity for fully-developed channel flow: comparison of modified model with wall functions (line) with data of Wei and Willmarth (symbols) at different Reynolds numbers.

V. FULLY-DEVELOPED CHANNEL FLOW

The model is implemented in the code PDF2DV[22] with the boundary conditions described above, and is tested for fully-developed channel flow. The model constants are

$$C_0=3.5; \quad C_{\omega 1}=0.44; \quad C_{\omega 2}=0.9; \qquad C_3=5.0; \quad C_4=0.25; \quad E=8.5. \tag{87}$$

The domain is discretized on a 40 cell grid, with 480 particles per cell. Results are compared with the DNS data set of Mansour for $Re_\tau=395$. For a channel halfwidth of 1.0, the conditions are imposed at $y_p=0.1$, which corresponds to $y^+=40$. Model profiles of mean velocity, turbulent kinetic energy, Reynolds shear stress, and dissipation are shown as the dashed lines in Figures 11 through 14, together with DNS data of Mansour (private communication). Generally good agreement is achieved for $\langle uv\rangle$, k, and ϵ, and for $\langle U\rangle$ in the logarithmic layer.

But the mean velocity is clearly underpredicted at the channel halfplane. This is associated with a deficiency in the ω model at the channel halfplane, previously pointed out by Minier.[29] The ω model is currently still under development as a general model to be used jointly with the pdf method.[15] The following modifications improve its performance in channel flow: The term

$$C_5 \frac{\langle u_i \omega\rangle}{k} \frac{\partial k}{\partial x_i} dt \tag{88}$$

is added to Eq. (13) with $C_5=1.4$. This term corresponds to part of the transport term which arises in the moment equations from the particle model for dissipation.[16] Also, Eq. (14) is changed to

$$S_\omega = C_{\omega 2} - C_{\omega 1}\frac{P}{\epsilon} + C_6 \max\left[0, 1-\frac{P}{\epsilon}\right]^3, \tag{89}$$

with

$$C_{\omega 1}=0.29; \quad C_{\omega 2}=0.75; \quad C_6=0.3. \tag{90}$$

It is not difficult to verify that the arguments of Section III for the constant and linear-stress layer are not undermined by the addition of these terms. However, these are ad-hoc modifications which restrict the applicability of this model to channel flows. They are included to allow us to demonstrate the viability of wall functions, and hopefully to provide some clues on what is required to give the ω model more general applicability. The profiles from the modified model are shown in the solid lines in Figures 11 through 14.

Velocity profiles and the friction coefficient for the modified model over varying Reynolds numbers are shown in Figs. 15 and 16. For each case, the chosen number of grid cells is proportional to the Reynolds number. The velocity profiles are compared to the experimental channel flow data of Wei and Willmarth[30] at Reynolds numbers $Re_h=14914$, 22776, and 39582, with Re_h based on the mean velocity at the channel halfplane and on the channel halfwidth. Based on previous work[18,30] these correspond to $Re_\tau=695$, 1012, and 1655, respectively. At these Reynolds numbers, the base model (not shown) performs adequately in the log layer and in much of the core region, but consistently underpredicts the

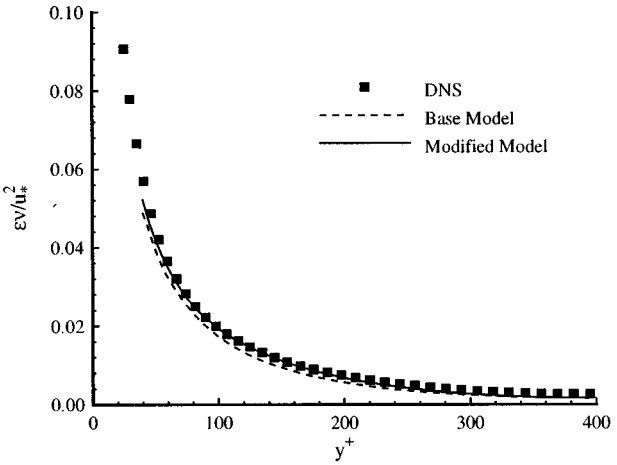

FIG. 14. Dissipation for fully-developed channel flow: comparison of models with wall functions (lines) with DNS data (symbols).

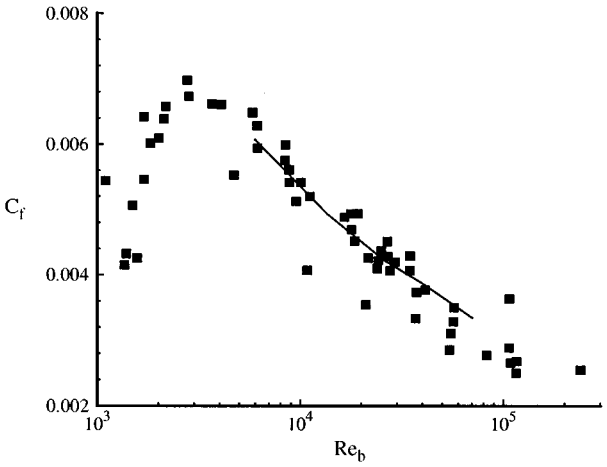

FIG. 16. Friction coefficient as a function of Reynolds number for fully-developed channel flow: comparison of modified model with wall functions (line) with data compiled by Dean.

halfplane mean velocity. Model results for the friction coefficient are compared with the experimental data compiled by Dean.[31] For halfplane mean velocity $\langle U\rangle_h$, the friction coefficient $C_f = \tau_w / \frac{1}{2}\rho\langle U\rangle_h^2$ is plotted against the Reynolds number Re_b, based on the bulk mean velocity and the full channel width. The modified model achieves plausible agreement at higher Reynolds numbers, and further demonstrates the viability of the wall-function boundary condition.

VI. CONCLUSION

A stable wall boundary condition is developed which reproduces the logarithmic velocity profile and shear stress in equilibrium flow conditions with the pdf method. Extension of traditional wall functions to include the additional information contained in the pdf is achieved by use of the self-similar Monte Carlo solution to the pdf evolution equation for the constant-stress layer. Accurate representation of the shear stress for flows at moderate as well as high Reynolds numbers is achieved through appeal to the linear-stress analysis for Reynolds stresses. Implementation with fully-developed channel flow shows successful use of the particle boundary conditions, but also points out aspects of the stochastic model for frequency which need further development. This work forms the basis for representing the effect of a solid wall in a turbulent reacting flow with the pdf method.

ACKNOWLEDGMENTS

We wish to thank Jean-Pierre Minier for useful discussions and insight. This work was supported by AFOSR Award No. F49620-93-1-0316.

[1] D. B. Spalding, *GENMIX — A General Computer Program for Two-Dimensional Parabolic Phenomena* (Pergamon Press, New York, 1977).
[2] B. E. Launder and D. B. Spalding, ''The numerical computation of turbulent flows,'' Comput. Methods Appl. Mech. Eng. **3**, 269 (1974).
[3] W. Rodi, *Turbulence Models and Their Application in Hydraulics — A State of the Art Review*, International Association for Hydraulic Research, Delft, 1980.
[4] A. K. Singhal and D. B. Spalding, ''Predictions of two-dimensional boundary layers with the aid of the $k-\epsilon$ model of turbulence,'' Comput. Methods Appl. Mech. Eng. **25**, 365 (1981).
[5] S. B. Pope and J. H. Whitelaw, ''The calculation of near-wake flows,'' J. Fluid Mech. **73**, 9 (1976).
[6] A. O. Demuren and S. Sarkar, ''Perspective: Systematic study of Reynolds-stress closure models in the computations of plane channel flows,'' J. Fluid Eng. **115**, 5 (1993).
[7] M. S. Anand, S. B. Pope, and H. C. Mongia, ''A Pdf method for turbulent recirculating flows,'' in *Turbulent Reactive Flows*, Lecture Notes in Engineering (Springer-Verlag, Berlin, 1989), pp. 672–693.
[8] A. S. Monin and A. M. Yaglom, *Statistical Fluid Mechanics* (MIT Press, Cambridge, 1971), Vol. I.
[9] J. O. Hinze, *Turbulence* (McGraw-Hill, New York, 1975).
[10] A. A. Townsend, *The Structure of Turbulent Shear Flows* (Cambridge University Press, Cambridge, 1976).
[11] S. B. Pope, ''Pdf methods for turbulent reactive flows,'' Prog. Energy Combust. Sci. **11**, 119 (1985).
[12] D. C. Haworth and S. B. Pope, ''A generalized Langevin model for turbulent flows,'' Phys. Fluids **29**, 387 (1986).
[13] S. B. Pope, ''On the relationship between stochastic Lagrangian models of turbulence and second-moment closures,'' Phys. Fluids **6**, 973 (1993).
[14] D. C. Wilcox, *Turbulence Modeling for CFD*, DCW Industries (La Cañada, CA, 1993).
[15] Jayesh and S. B. Pope, ''Stochastic model for turbulent frequency,'' Technical Report FDA-95-05, Cornell University, Ithaca, NY, October 1995.
[16] S. B. Pope and Y. L. Chen, ''The velocity–dissipation probability density function model for turbulent flows,'' Phys. Fluids A **2**, 1437 (1990).
[17] N. Wax, *Noise and Stochastic Processes* (Dover, New York, 1954).
[18] T. D. Dreeben and S. B. Pope, ''Pdf and Reynolds-stress modeling of near-wall turbulent flows,'' Phys. Fluids **9**, 154 (1997).
[19] T. D. Dreeben, ''Pdf modeling of near-wall turbulent flows,'' Ph.D. thesis, Cornell University, Ithaca, NY, 1996.
[20] B. E. Launder, G. J. Reece, and W. Rodi, ''Progress in the development of a Reynolds-stress turbulence closure,'' J. Fluid Mech. **68**, 537 (1975).
[21] S. B. Pope, ''Application of the velocity-dissipation probability density function model to inhomogeneous flows,'' Phys. Fluids A **3**, 1947 (1991).
[22] S. B. Pope, PDF2DV, 1994, A Fortran code to solve the modelled joint Pdf equations for two-dimensional recirculating flows (Cornell University, unpublished).
[23] F. Durst, J. Jovanovic, and L. J. Kanevce, ''Probability density distribution in turbulent wall boundary-layer flows,'' in *Turbulent Shear Flows 5* (Springer-Verlag, Berlin, 1987).
[24] F. Durst, J. Jovanovic, and J. Sender, ''LDA measurements in the near-wall region of a turbulent pipe flow,'' J. Fluid Mech. **295**, 305 (1995).
[25] P. K. Yeung and S. B. Pope, ''Lagrangian statistics from direct numerical simulations of isotropic turbulence,'' J. Fluid Mech. **207**, 531 (1989).
[26] N. N. Mansour (private communication, 1994).
[27] P. G. Huang and P. Bradshaw, ''Law of the wall for turbulent flows in pressure gradients,'' Am. Inst. Aeronaut. Astronaut. J. **33**, 624 (1995).
[28] S. B. Pope, ''Modified wall functions for PDF/Monte Carlo particle methods,'' Cornell University, Ithaca, NY, 1992.
[29] J. P. Minier (private communication, 1996).
[30] T. Wei and W. W. Willmarth, ''Reynolds-number effects on the structure of a turbulent channel flow,'' J. Fluid Mech. **204**, 57 (1989).
[31] R. B. Dean, ''Reynolds number dependence of skin friction and other bulk flow variables in two-dimensional rectangular duct flow,'' J. Fluid Eng. **100**, 215 (1978).